Journal of Electroceramics, 7, 95–105, 2001

The Effect of the Oxygen Exchange at Electrodes on the High-Voltage Electrocoloration of Fe-Doped $SrTiO_3$ Single Crystals: A Combined SIMS and Microelectrode Impedance Study

S. RODEWALD,[1] N. SAKAI,[2] K. YAMAJI,[2] H. YOKOKAWA,[2] J. FLEIG[1,*] & J. MAIER[1]

[1]*Max Planck Institut für Festkörperforschung, Heisenbergstr. 1, 70569 Stuttgart, Germany*
[2]*National Institute of Materials and Chemical Research, Ibaraki 305-8565, Japan*

Submitted December 27, 2000; Revised June 15, 2001; Accepted June 22, 2001

Abstract. The effect of the electrode material on the high voltage stoichiometry-polarization ("electrocoloration") of Fe-doped $SrTiO_3$ single crystals has been studied. For different electrode materials (150-nm Ag/15-nm Cr and 150-nm Au/15-nm Cr) secondary ion mass spectrometry (SIMS) was used to measure the depth profile of the ^{18}O-isotope after high-field stress. The results were compared with spatially resolved impedance measurements on electrocolored Fe-doped $SrTiO_3$ single crystals. For Au/Cr as well as Ag/Cr electrodes a large dc voltage leads to moving color fronts which are usually correlated with a pronounced stoichiometry polarization of the samples due to electrodes blocking the ionic current. However, the local impedance measurements demonstrate that the conductivity profiles near the cathode depend on the electrode material. This finding is in accordance with the SIMS measurements which indicate that the Ag/Cr-electrodes are, in contrast to Au/Cr-electrodes not completely inactive for the oxygen incorporation into the Fe-doped $SrTiO_3$. The results are discussed in terms of defect chemical models.

Keywords: strontium titanate, electrocoloration, impedance spectroscopy, SIMS, oxygen exchange

1. Introduction

The resistance degradation of electroceramics at high voltages (electrocoloration) has been studied for many years particularly on acceptor doped $SrTiO_3$ [1–3] and $BaTiO_3$ [4, 5]. The degradation could be assigned to stoichiometry changes in the material [1, 2] similar to a conventional Wagner–Hebb polarization [6, 7]. To achieve such a stoichiometry polarization at least one of the electrodes used for electrocoloration has to be strongly blocking for ionic current. For different electrode materials (Al [3], Ag [5], Au [1, 2] and Pt [8]) electrocoloration has been observed and hence all these metals have been assumed to be almost completely inactive with respect to the oxygen exchange at the oxide/electrode interface.

On the other hand, on ZrO_2 or CeO_2 solid electrolytes Ag-electrodes turned out to be much less blocking with respect to the oxygen reduction reaction than Au-electrodes [9–13]. Owing to the relative high solubility of oxygen and the non-negligible oxygen diffusion coefficient in Ag [10, 14–18] even in the case of a dense Ag-electrode a certain oxygen reduction rate can be measured [17]. Hence one could expect that, although electrocoloration can be observed for different metal electrodes, the shape of the stoichiometry and conductivity profiles inside the samples might depend on the kind of electrodes used. In previous works [2, 19] microcontact impedance spectroscopy has been used to study the conductivity profiles in single- and poly-crystalline Fe-doped $SrTiO_3$ electrocolored by means of Au/Cr-electrodes, and the data could be quantitatively related to stoichiometry profiles inside the samples.

In this contribution, two different techniques were applied to study the effect of the electrode material (Ag, Au) on the electrocoloration process: (a) microcontact impedance spectroscopy was used to measure the conductivity profiles inside the samples caused by the electrocoloration and (b) secondary ion mass spectrometry

*To whom all correspondence should be addressed.

(SIMS) experiments were performed to investigate the ^{18}O-isotope incorporation at the electrodes during electrocoloration. Numerical calculations simulating the stoichiometry changes in the samples during the electrocoloration process are used to interpret the experimental results obtained for Ag- and Au-electrodes.

2. Defect Chemistry in Fe-Doped $SrTiO_3$

Owing to their importance as electroceramic materials the defect chemistry of $SrTiO_3$ and $BaTiO_3$ has been investigated in great detail [20–24]. The native disorder is of Schottky type but the defect concentrations in the material are in most cases dominated by the presence of acceptors (Fe, Mn, Ni, etc.) or donors (La, V, Mo, etc.) on the A- or B-sites of the perovskite lattice. The defect chemical relations valid for Fe-doped $SrTiO_3$ are given by the following equations:

$$O_O^{\times} + Sr_{Sr}^{\times} \rightleftharpoons V_{Sr}^{||} + V_O^{\bullet\bullet} + \text{''SrO''}$$

partial Schottky equilibrium (1)

$$1/2O_2 + V_O^{\bullet\bullet} \rightleftharpoons O_O^{\times} + 2h^{\bullet}$$

oxygen exchange (2)

$$\text{nil} \rightleftharpoons e^{|} + h^{\bullet}$$ band-band-interaction (3)

$$Fe_{Ti}^{\times} \rightleftharpoons Fe_{Ti}^{|} + h^{\bullet}$$ trapping reaction (4)

$$2\left[V_O^{\bullet\bullet}\right] + [h^{\bullet}] = [e^{|}] + \left[Fe_{Ti}^{|}\right]$$

charge neutrality (5)

$$[Fe] = \left[Fe_{Ti}^{|}\right] + \left[Fe_{Ti}^{\times}\right]$$

mass conservation of dopant (6)

3. Experimental

3.1. Preparation of Samples

For all measurements presented in this contribution Fe-doped $SrTiO_3$ single crystals with a nominal doping of 0.13 wt% (Frank & Schulte GmbH, Essen, Germany) have been used. The samples (square slices of $6 \times 6\ mm^2$ with a thickness of 1 mm) were cut from the crystal boule with a diamond saw. The surfaces were lapped and polished with Syton (30%-SiO_2/13%-Na_2O/H_2O; pH = 10.2; particle size = 0.125 μm) to optical quality. All samples were equilibrated in a high temperature furnace (Gero GmbH, Germany) in air at 1000 K for 8 h to achieve a well-defined homogeneous distribution of the mobile charge carriers. The electrodes (nominally 150-nm Ag/15-nm Cr or 150 nm-Au/15-nm Cr) were evaporated on the samples. The thin 15-nm Cr-layer is necessary to improve the adhesion of the Au- or Ag-layer to the $SrTiO_3$-surface. The electrode geometries used are shown in Fig. 1: Stripe-like (Fig. 1(a)) and quadratic (Fig. 1(b)) electrodes were used for the electrocoloration process (high-field stress), while an array of several thousand circular microelectrodes with a diameter and spacing of 10 μm (Fig. 1(a)) prepared by lithographical techniques has been employed to measure the local conductivity profile after electrocoloration. Sketches of the sample's geometries used for the spatial conductivity experiments and the SIMS measurements are shown in Fig. 1(a) and (b), respectively.

3.2. Electrocoloration of the Samples

3.2.1. In air. $SrTiO_3$-samples with stripe electrodes (Fig. 1(a)) were electrocolored in air at 493 K. The stripe electrodes were contacted with tungsten tips via micromanipulators and connected to a high voltage source and measuring unit (Model 237, Keithley). The electrocoloration was performed for 90 min at a dc voltage of 300 V. The samples were quenched to room temperature immediately after the voltage was turned off. On these electrocolored samples conductivity profiles were measured by means of microelectrodes (see below).

3.2.2. In ^{18}O-atmosphere. The electrocoloration of samples later used for the SIMS experiments (Fig. 1(b)) were carried out in an ^{18}O-atmosphere in a gas tight sample holder with a gas inlet and outlet as shown in Fig. 2. The sample was electrically connected to a Potentiostat/Galvanostat (Model 2020, Toho Giken Co. Ltd., Japan) with two lead-in wires and placed inside a glasswool covered Pt-basket at the bottom of the sample holder. A high heating and cooling rate of the sample before and after electrocoloration was achieved by using an infrared furnace (MR39H, Shinku-Riko Co. Japan). The temperature of the sample was monitored with a Pt/Pt-3%Rh thermocouple. The gas circulation system to exchange the gas atmosphere in the sample holder is described in Ref. [25]. After evacuation the system was filled with an 97% $^{18}O_2$-isotope enriched (Isotec Co. Ltd., USA) atmosphere of 200 mbar. The

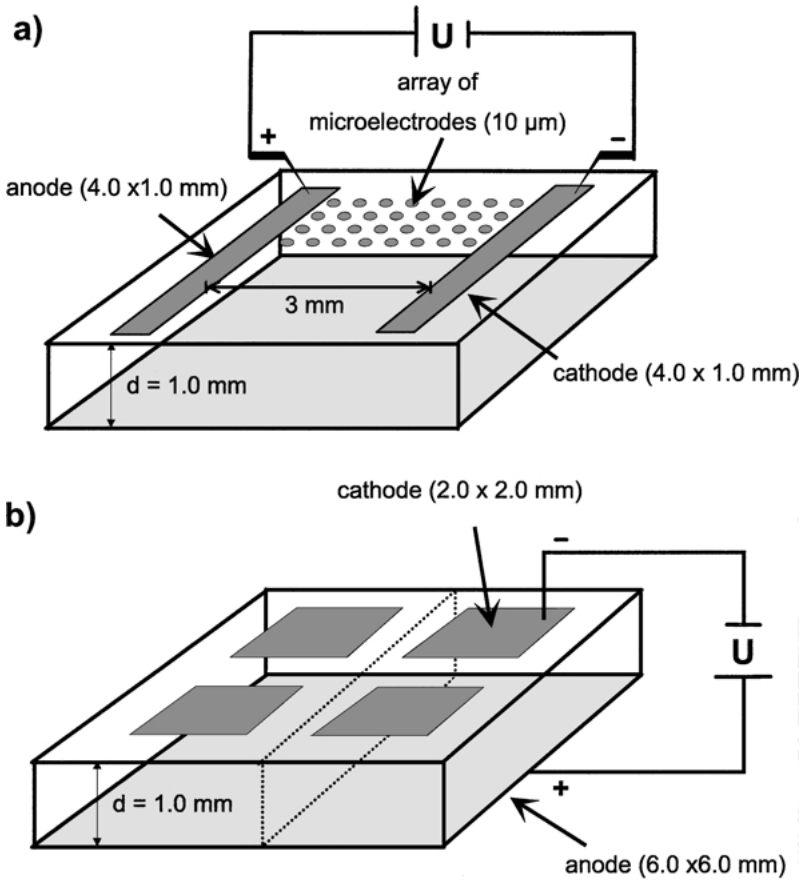

Fig. 1. Sketches of the electrode geometries used for (a) microcontact-impedance measurements (the microelectrodes are magnified, their number is much larger than shown) and (b) SIMS-analysis of electrocolored Fe-doped $SrTiO_3$-single crystals. For some samples investigated by SIMS-analysis only half of the shown geometry as indicated by the dotted line has been used.

exchange temperature of 473–673 K was reached in less than 5 min and a voltage of 100 V was applied to the sample for 7 s to 60 min. The electrocoloration time was usually choosen such that the expected extension of the dark color front (estimated by finite difference calculations) was essentially temperature independent. After electrocoloration the sample was rapidly cooled down to room temperature.

3.3. Microcontact Impedance Measurements

The setup to perform the microcontact impedance measurements is shown in Fig. 3. The sample is placed on an electrically insulating 3-mm thick sapphire plate located on a hot chuck and is heated to about 415 K. At this measurement temperature the diffusion processes in the sample are still slow enough to keep the shape of stoichiometry profiles stable for several hours [19] and therefore reasonable conductivity profile measurements were possible. Two tungsten tips moved by micromanipulators were used to electrically contact a circular microelectrode and a stripe counter electrode on the Fe-doped $SrTiO_3$ surface, respectively. The impedance was measured between these two electrodes using a frequency response analyzer (Solartron 1260, Schlumberger) in combination with a home made high impedance converter. From the high frequency (bulk) semicircle of the obtained impedance spectra the local bulk conductivities (σ_{bulk} = sum of ionic and electronic bulk conductivity) were calculated according to the spreading resistance formula $R = (\sigma_{\text{bulk}} \cdot 2 \cdot d)^{-1}$ (d = microelectrode diameter) [26]. Subsequent contacting microelectrodes in a line yield conductivity profiles with a spatial resolution of about 20 μm. More information with respect to such measurements is given in [2, 19].

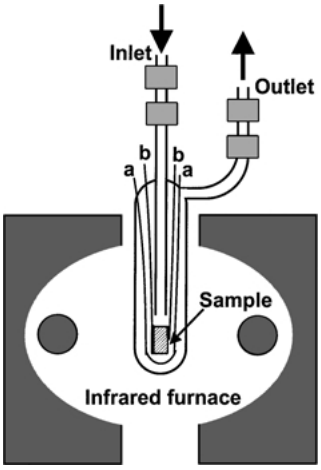

Fig. 2. Schematic picture of the sample holder used for the electrocoloration of the samples under an $^{18}O_2$-atmosphere. The sample holder has two pairs of wires: (a) Pt/Pt-3% Rh thermocouple, (b) leading wires for the electrocoloration.

3.4. Sims-Analysis

The SIMS analysis was performed by using a setup (ims5f, CAMECA Instruments, France) with a Cs^+ primary ion beam at an accelerating voltage of 10 kV. The isotope exchange and element distribution profiles were measured at electrode and at free surface regions at different temperatures by the depth profiling mode. Therefore a large primary ion beam (150 μm $\times$ 150 μm) was used to sputter craters into the samples. The depth of the crater was determined by a surface profilometer (Dektak^3, Veeco/Sloan Co. Ltd., USA) and correlated with the sputtering time by assuming a constant sputtering rate during the SIMS measurement.

4. Results and Discussion

4.1. Microcontact Impedance Measurements

Figure 4 shows two conductivity profiles in Fe-doped $SrTiO_3$ single crystals obtained after electrocoloration at 493 K with different electrode materials. The profile in Fig. 4(a) was measured at 417 K after electrocoloration with Au/Cr and the profile in Fig. 4(b) displays the data obtained with Ag/Cr-electrodes at 413 K. Both profiles have a very characteristic shape with a regime of enhanced conductivity towards the anode side and a sharp minimum close to the dark color front. However only the sample electrocolored with Au/Cr-electrodes shows a conductivity increase at the cathodic side. The profile in Fig. 4(a) can be quantitatively interpreted in terms of a stoichiometry polarization with two ionically blocking electrodes [19]: The anodic increase can be attributed to a hole conduction regime and the dip reflects a change of the conduction mechanism from hole to ionic conduction due to a sharp increase of the

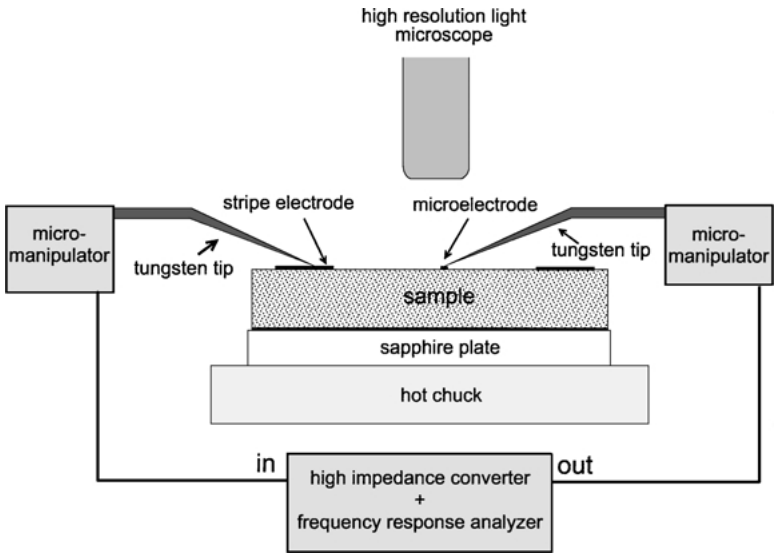

Fig. 3. Sketch of the set-up used for the microcontact-impedance measurements.

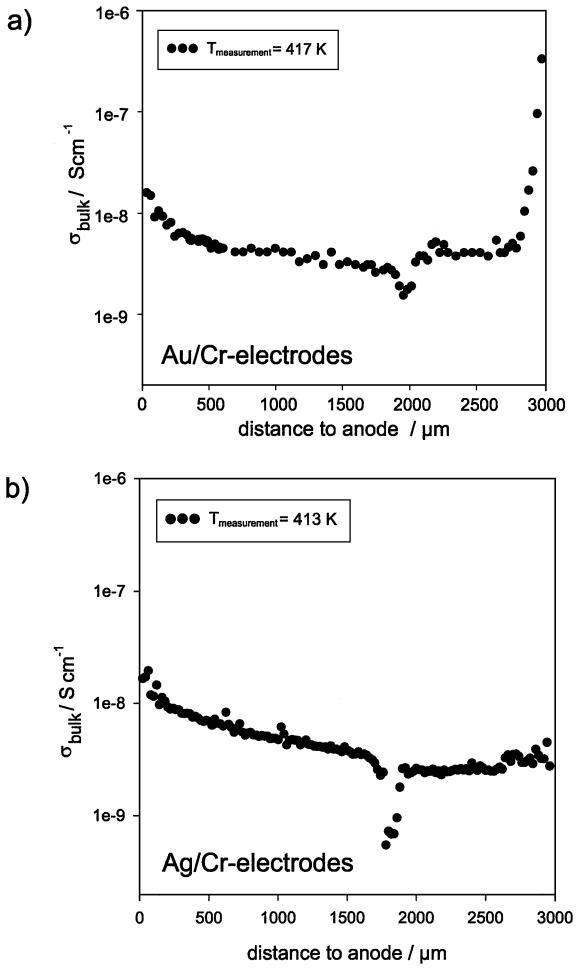

Fig. 4. Measured bulk conductivity profiles in the electrocolored (T_{elec} = 493 K, t_{elec} = 90 min, U_{elec} = 300 V) samples using (a) Au/Cr- and (b) Ag/Cr-electrodes. The conductivity values have been calculated from the resistance of the high frequency semicircle in the impedance plot.

ionic charge carrier concentration in this region. The enhancement at the cathode, finally, is caused by an increased electron concentration due to a pile up of the oxygen vacancies at the ion blocking Au/Cr/$SrTiO_3$ interface [1, 19].

The differences in the conductivity profiles at the cathode side suggest that the blocking effect of the Ag/Cr-electrode with respect to the ionic charge carriers is less pronounced than for the Au/Cr-electrode. However, for a sound interpretation it is necessary to know how a partial permeability of the electrode would influence the entire profile. Mass action constants of Eqs. (1)–(4) as well as the mobilities of the charge carriers are reported in literature [23, 24] and a finite-difference algorithm based on the defect chemical relations (Eqs. (1)–(6)) can be used to simulate the time-dependent defect concentration profiles in Fe-doped $SrTiO_3$ single crystals during the electrocoloration. Details on such calculations are given in Ref. [1, 19, 27]. Here the case of partial reversibility at the electrodes is considered, i.e. a certain oxygen incorporation and excorporation at the electrodes is taken into account. Since an exact description of the concentration and potential dependence of the oxygen exchange at the cathode is not available the following model was used to qualitatively take account of the partial reversibility: It was assumed that during the electrocoloration a certain fraction f_c of the oxygen vacancy flux entering the n-th element $J_{V_{n-1/n}}$ (facing the cathode, see Fig. 5) leaves the sample at the cathode/electrolyte interface ($J_{V_{cathode}} = f_c\, J_{V_{n-1/n}}$) while a certain fraction f_A of the oxygen vacancy flux leaving the first element ($J_{V1/2}$) enters the sample at the anode ($J_{V_{anode}} = f_A \cdot J_{V1/2}$).

If about 60% of $J_{V_{n-1/n}}(J_{V_{1/2}})$ leaves (enters) the sample both the cathodic and the anodic conductivity enhancements are almost equivalent as obtained for totally blocking electrodes (Fig. 6(a) and (b)) and as measured for the Au/Cr-electrode (Fig. 4(a)). If, on the other hand $f_A = f_C = 0.8$ the cathodic conductivity enhancement almost vanishes while the anodic enhancement only slightly decreases (Fig. 6(c)). The profile for $f_A = f_C = 0.8$ corresponds to the experimentally observed profile in the sample with Ag/Cr-electrodes and supports the assumption that the Ag/Cr-electrodes, though leading to an electrocoloration and conductivity enhancement at the anode, are far from being completely ionically blocking. From the conductivity enhancement at the anode it can not even be concluded that the anode is completely ionically blocking since a partial blocking is

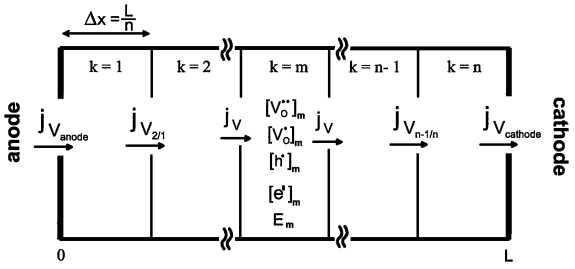

Fig. 5. Schematic model used to calculated the conductivity profiles for electrocolored samples by assuming totally and partially blocking electrode interfaces.

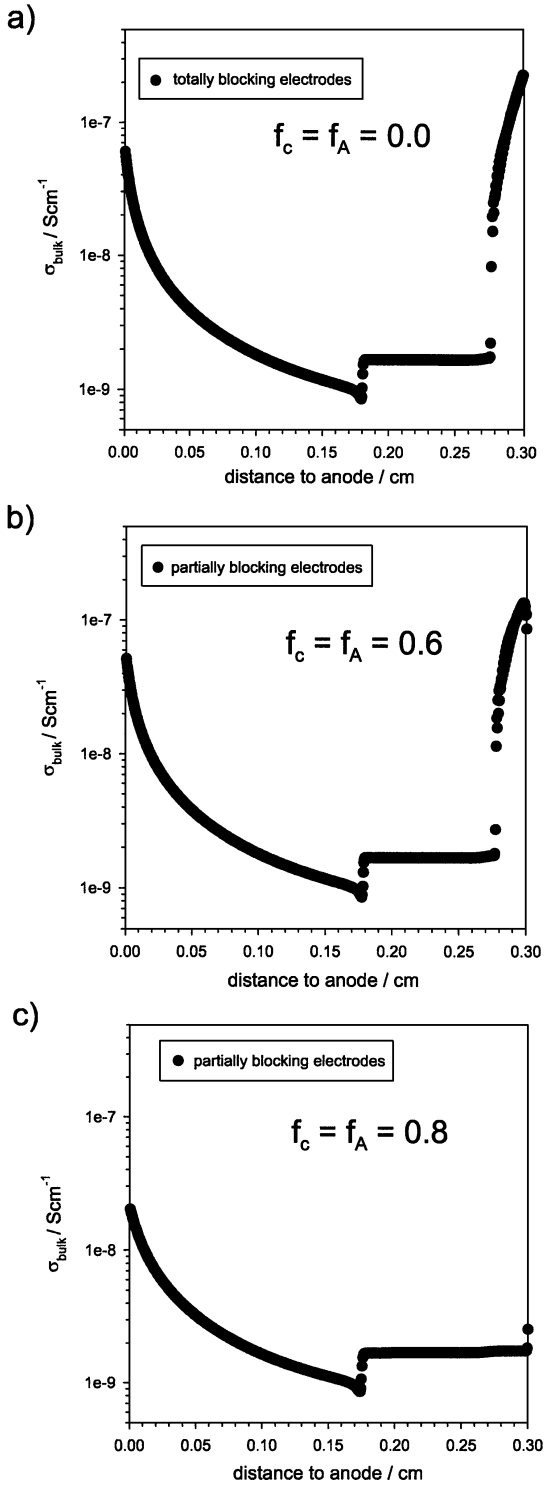

Fig. 6. Conductivity profile calculated for electrocolored samples by assuming (a) totally blocking ($f_C = f_A = 0.0$), (b) ($f_C = f_A = 0.6$) and (c) ($f_C = f_A = 0.8$) partially blocking electrode interfaces.

sufficient to yield the measured profile and hence the electrocoloration.

These calculations show that the assumption of a certain oxygen exchange at the Ag/Cr-electrode can easily explain the different conductivity profiles measured with different electrode materials. This assumption is also supported by experiments on ZrO_2 or CeO_2 electrolytes ([9–12], see also Introduction) which report an enhanced electrochemical activity of the Ag-electrode. However, to further check in how far an enhanced oxygen incorporation rate at the Ag/Cr-electrodes can be observed on $SrTiO_3$, additional SIMS-experiments have been performed after electrocoloration in $^{18}O_2$-atmosphere.

4.2. Sims Analysis

4.2.1. Element distribution. Figure 7 shows the in-depth distribution profiles of the most common elements measured from the surface of the (a) Au/Cr- and (b) Ag/Cr-cathode into the electrocolored $SrTiO_3$ single crystal. Because of the weak intensity of the monitored M^--ion counts (M^-), MO^--ion counts (MO^-) have been monitored. The profiles show that the ratios of (^{88}SrO)/(^{48}TiO) and (^{18}O) and (^{16}O) in the bulk are nearly constant and that the (^{18}O)/(^{16}O)-ratio exhibits the expected element ratio. This implies that the samples have a very homogeneous element distribution in the bulk, which is essential for the further interpretation of the results obtained by SIMS-analysis. The distribution profiles of (^{18}O) normalized to the total oxygen counts ((^{18}O) + (^{16}O)) measured from the electrode covered parts and the free surfaces into the Fe-doped $SrTiO_3$ will be discussed in more detail.

4.2.2. Samples with Au/Cr-electrodes. Depth profiles of the frozen-in ^{18}O-isotope concentrations measured at the Au/Cr-cathodes of Fe-doped $SrTiO_3$ single crystals electrocolored at different temperatures (473–673 K) are shown in Fig. 8. Only a very shallow ^{18}O-concentration profile could be detected up to 50 nm into the 150 nm thick Au-layer. This profile could not be fitted with a diffusion profile and is possibly due to ion beam mixing effects within the first 50 nm. No ^{18}O-concentration profile could be detected underneath the electrode layer inside the Fe-doped $SrTiO_3$. Therefore the Au/Cr-cathodes can be assumed to be almost completely blocking for the

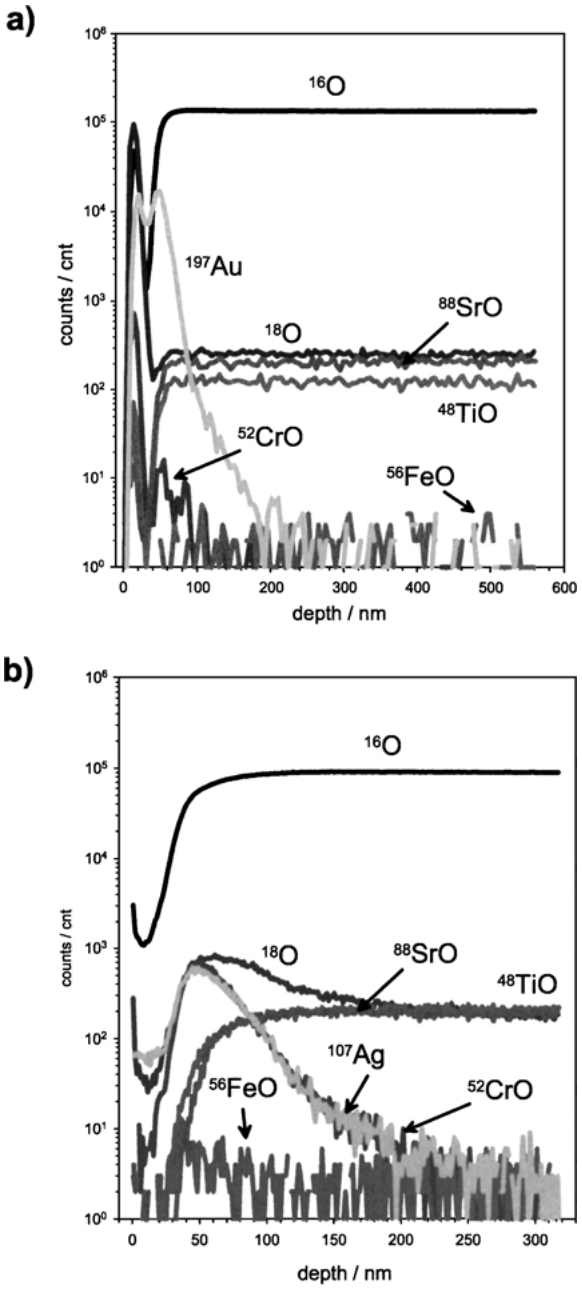

Fig. 7. Typical element distribution profiles measured by SIMS from the (a) Au/Cr- and (b) Ag/Cr-electrode surface into the Fe-doped $SrTiO_3$-single crystals.

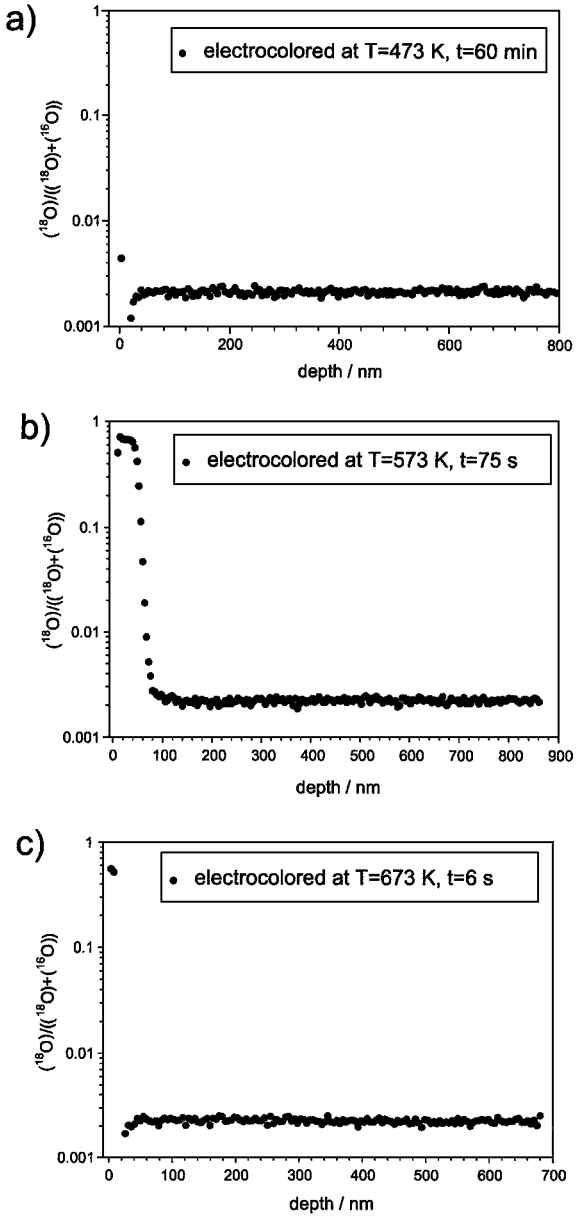

Fig. 8. Normalized ^{18}O-concentration profiles measured from the Au/Cr-cathodes into the Fe-doped $SrTiO_3$-single crystals after electrocoloration at three different temperatures (a) 473 K, (b) 573 K and (c) 673 K.

oxygen incorporation within the investigated temperature regime (473–673 K). Depth-profiles obtained at the free $SrTiO_3$ surfaces (see Fig. 9(a)) show also a very shallow (<40 nm) ^{18}O-concentration profile. This does again not seem to be a diffusion profile, in view of the independency of the penetration depth from annealing time. It might be due to some ion beam mixing effects or a thin surface layer (<40 nm) which exchanges oxygen with the surrounding gas atmosphere. These results verified the assumption used for the finite-difference calculations of the defect concentration profiles in

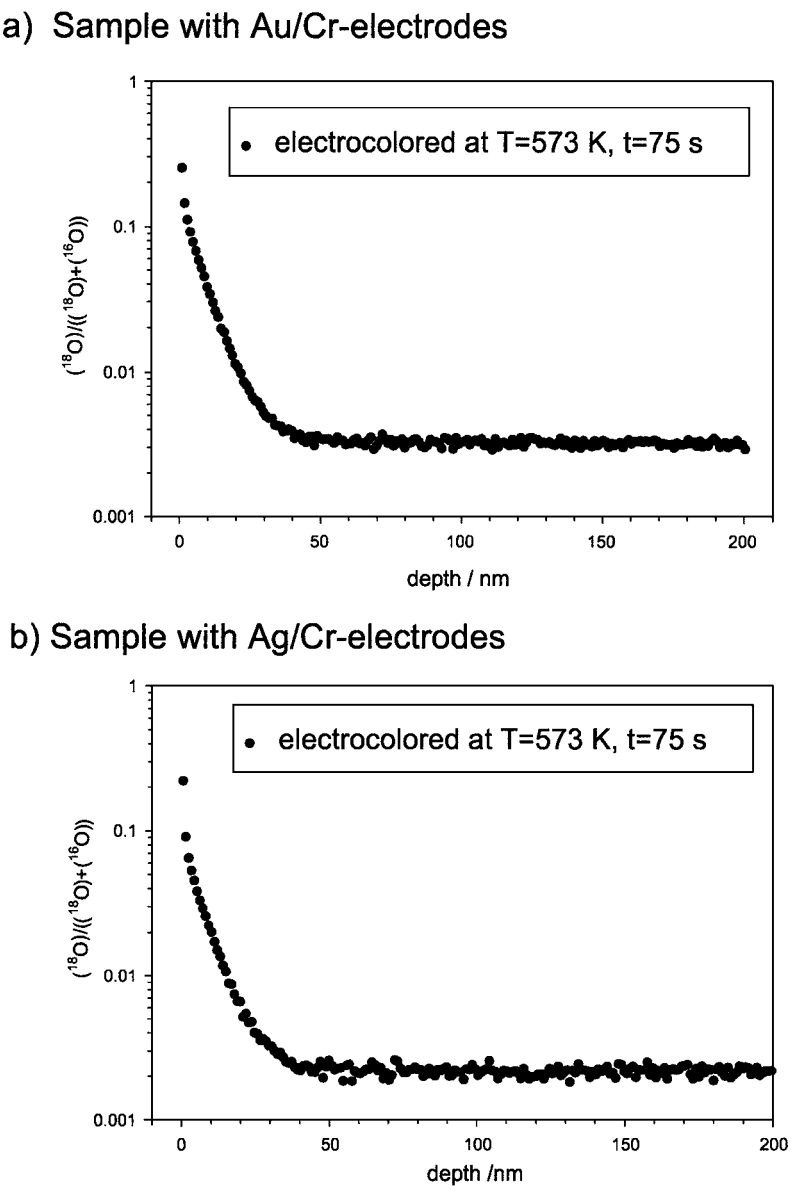

Fig. 9. Normalized ^{18}O-concentration profiles measured from the free Fe-doped $SrTiO_3$-surface into the sample. The samples had been electrocolored with (a) Au/Cr- and (b) Ag/Cr-electrodes at 573 K.

the electrocolored samples that no significant oxygen-exchange with the surrounding atmosphere takes place during the electrocoloration. The results obtained by SIMS-analysis on Fe-doped $SrTiO_3$-single crystals electrocolored with Au/Cr-electrodes are therefore in accordance with the microcontact impedance measurements discussed above (Fig. 4(a)) and imply that nearly no oxygen incorporation neither at the free surfaces nor at the electrode/electrolyte interface took place during electrocoloration within the investigated temperature range.

4.2.3. Samples with Ag/Cr-electrodes. The depth profiles measured at the free $SrTiO_3$ surfaces of the samples electrocolored with Ag/Cr-electrodes (see Fig. 9(b)) were almost the same as those measured in the samples with Au/Cr-electrodes. No oxygen incorporation in a depth larger than 40 nm took place.

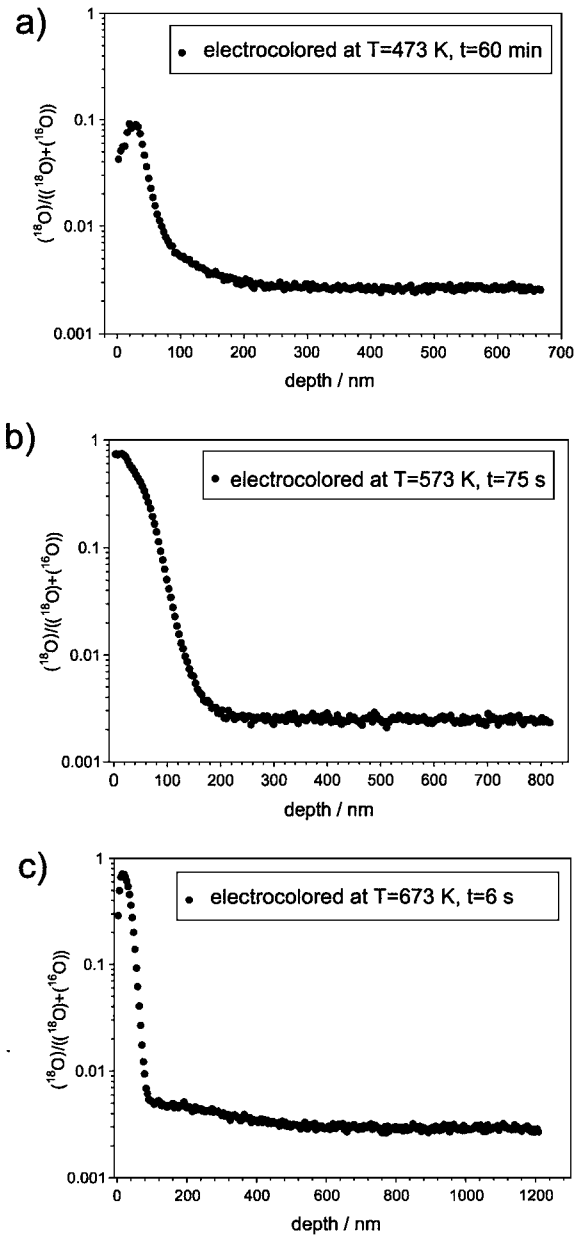

Fig. 10. Normalized ^{18}O-concentration profiles measured from the Ag/Cr-cathodes into the Fe-doped $SrTiO_3$-single crystals after electrocoloration at three different temperatures (a) 473 K, (b) 573 K and (c) 673 K.

However the ^{18}O-concentration profiles measured at the Ag/Cr-cathodes (Fig. 10) show that during electrocoloration a distinct ^{18}O-incorporation into the Ag/Cr-electrode layer occured and that to some extent ^{18}O was also incorporated into the Fe-doped $SrTiO_3$-single crystal underneath the approximatly 165-nm thick electrode layer. In particular at 673 K (Fig. 10(c)) a ^{18}O-depth of several 100 nm is observed indicating a considerable incorporation into the $SrTiO_3$. In this context it has to be mentioned that a different sputtering behaviour of metals and oxides, due to more pronounced charging effects at the oxide compared to the metal surface, has to be expected. Therefore the assumption of a constant sputtering rate—which is used to correlate sputtering depth and sputtering time—is only an approximation. By taking this into account the sharp bend in Fig. 10(c) (at ca. 80 nm) might indicate the transition from the Ag/Cr-electrode to $SrTiO_3$. The ^{18}O-depth profiles in the samples electrocolored at lower temperatures (473 K and 573 K) also exceed the thickness of the electrode layer.

Further measurements have been carried out to investigate the relation between the ^{18}O-penetration depth and the electrocoloration time at a constant temperature (573 K). With increasing electrocoloration time a considerable increase of the ^{18}O-penetration depth is achieved (Fig. 11). However, it has to be taken into account that morphological changes of the electrode layer took place during the electrocoloration increasing the porosity of the Ag/Cr-electrode considerably. In the case of a very high ^{18}O-incorporation into the Fe-doped $SrTiO_3$ (600 s of electrocoloration, Fig. 11(c)) the Ag/Cr-cathode turned out to be highly porous after electrocoloration while after smaller electrocoloration times the Ag/Cr-cathodes were less porous (Fig. 11(a) and (b)). Morphological changes are much less pronounced in the case of Ag/Cr-electrodes which have not been used for electrocoloration even if they pass through the same thermal history. For such "untreated" electrodes the observed ^{18}O-incorporation was also much less pronounced.

It can, in summary, be concluded that electrocoloration with Ag/Cr-electrodes leads to an incorporation of ^{18}O in $SrTiO_3$ and that, probably due to the increased three-phase boundary length (O_2, Ag, $SrTiO_3$), morphological changes further enhance this incorporation. (The role of the thin and possibly porous Cr-layer with respect to the oxygen incorporation kinetics has not been investigated in more detail.) The measurements presented here therefore demonstrate that the electrode material can have a strong effect on the high-field stoichiometry polarization of $SrTiO_3$ and that this effect can consistently be explained by the different

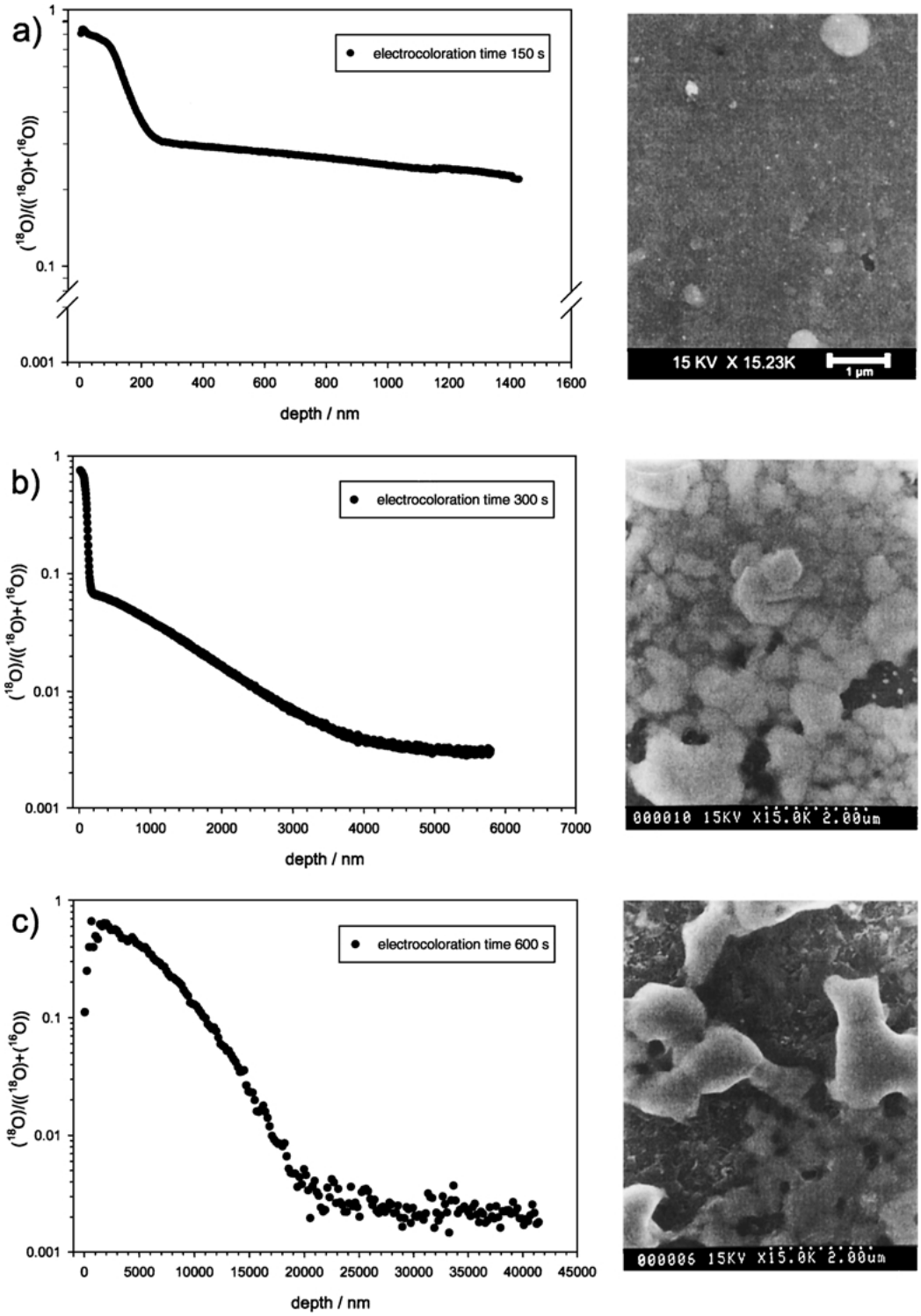

Fig. 11. Normalized ^{18}O-concentration profiles measured from the Ag/Cr-cathodes into the Fe-doped $SrTiO_3$-single crystals after electrocoloration at 573 K for three different times (a) 150 s, (b) 300 s and (c) 600 s) and SEM-images of the corresponding Ag/Cr-electrode layers.

oxygen incorporation rates of Ag/Cr and Au/Cr-electrodes.

5. Conclusion

Fe-doped $SrTiO_3$ single crystals electrocolored by using Au/Cr- and Ag/Cr-electrodes show the same color front movement during the high field stress. However, the conductivity profiles in the electrocolored $SrTiO_3$-samples depend on the electrode material: An enhanced conductivity as found near Au/Cr-cathodes could not be detected in the vicinity of the Ag/Cr-cathode. Finite-difference calculations of the electrocoloration process show that conductivity profiles as measured with Ag/Cr-electrodes can be expected for partly permeable electrode/$SrTiO_3$-interfaces.

Results obtained by SIMS-analysis of Fe-doped $SrTiO_3$ single crystals electrocolored with Ag/Cr- and Au/Cr-electrodes in $^{18}O_2$-atmosphere support these observations. Nearly no oxygen exchange during electrocoloration could be detected for the samples with Au/Cr-electrodes between 473–673 K hence supporting the assumption of almost completely blocking electrodes (with respect to ions). For Ag/Cr-electrodes, on the other hand, an incorporation of ^{18}O into the Ag/Cr-layer and to some extent also into the $SrTiO_3$ underneath the Ag/Cr-cathode could be detected. Therefore these electrodes are partially permeable for ions.

These measurements exemplarily demonstrate that the electrode materials can considerably influence the high field stoichiometry polarization in oxides although the color front movement does not reflect these differences.

Acknowledgments

The financial support of the research stay of Stefan Rodewald at the National Institute for Materials and Chemical research in Tsukuba, Japan by a STA-Fellowship of JISTEC is gratefully acknowleged.

References

1. T. Baiatu, R. Waser, and K.-H. Härdtl, *J. Am. Ceram. Soc.*, **73**, 1663 (1990).
2. S. Rodewald, J. Fleig, and J. Maier, *J. Eur. Ceram. Soc.*, **19**, 797 (1999).
3. J. Blanc and D.L. Staebler, Phys. *Rev.* B **4**, 3548 (1971).
4. J. Rödel and G. Tomandl, *J. Mat. Sci.*, **19**, 3515 (1984).
5. W.A. Schulze, L.E. Cross, and W.R. Buessem, *J. Am. Ceram. Soc.*, **63**, 83 (1980).
6. M.H. Hebb, *J. Chem. Phys.*, **20**, 185 (1952).
7. I. Yokota, *J. Phys. Soc. Japan*, **16**, 2213 (1961).
8. R. Waser, T. Baiatu, and K.-H. Härdtl, *J. Am. Ceram. Soc.*, **73**, 1654 (1990).
9. R. Baker, J. Guindet, and M. Kleitz, *J. Electrochem. Soc.*, **144**, 2427 (1997).
10. J. Van Herle and A.J. McEvoy, *J. Phys. Chem. Solids*, **55**, 339 (1994).
11. M.Gödickemeier, K. Sasaki, L.J. Gauckler, and I. Riess, *J. Electrochem. Soc.*, **144**, 1635 (1997).
12. D.Y. Wang and A.S. Nowick, *J. Electrochem. Soc.* **128**, 55 (1981).
13. B.A. van Hassel, B.A. Boukamp, and A.J. Burggraaf, *Solid State Ionics*, **48**, 139 (1991).
14. T.A. Ramanarayanan and R.A. Rapp, *Metall. Trans.*, **3**, 3239 (1972).
15. S.P.S. Badwal, M. Bannister, and M. Murray, *J. Electroanal. Chem.*, **168**, 363 (1984).
16. H. Rieckert and R. Steiner, *Z. Phys. Chem. NF*, **49**, 127 (1966).
17. F.K. Moghadam and D.A. Stevenson, *J. Electrochem. Soc.*, **133**, 1329 (1986).
18. R. Jiminez, T. Kloidt, and M. Kleitz, *J. Electrochem. Soc.*, **144**, 582 (1997).
19. S. Rodewald, J. Fleig, and J. Maier, *J. Am. Ceram. Soc.*, **83**, 1969 (2000).
20. J. Daniels, K.-H. Härdtl, and R. Wernicke, *Phil. Tech. Rev.*, **38**, 73 (1978).
21. H. Okinaka and T. Hata, *Am. Ceram. Soc. Bull.*, **74**, 62 (1995).
22. N. Yamaoka, *Ceram. Bull.*, **65**, 1149 (1996).
23. I. Denk, W. Münch, and J. Maier, *J. Am. Ceram. Soc.*, **78**, 3265 (1995).
24. R. Moos and K.-H. Härdtl, *J. Am. Ceram. Soc.*, **80**, 2549 (1997).
25. T. Kawada, K. Masuda, J. Suzuki, A. Kaimai, Y. Nigara, J. Mizusaki, H. Yugami, H. Arashi, N. Sakai, and H. Yokokawa, *Solid State Ionics*, **121**, 271 (1999).
26. J. Newman, *J. Electrochem. Soc.*, **113**, 501 (1966).
27. T. Baiatu, "A model to describe the degradation of $SrTiO_3$ poly- and single-crystals under dc voltage stress," Ph.D. Thesis, University of Karlsruhe, Karlsruhe, Germany (1988).